ACS Catalysis

Research Article

pubs.acs.org/acscatalysis

How Surface Hydroxyls Enhance MgO Reactivity in Basic Catalysis: The Case of Methylbutynol Conversion

Hugo Petitjean,*[,†] Hazar Guesmi,*[,†,‡,§] Hélène Lauron-Pernot,[‡,§] Guylène Costentin,[‡,§] David Loffreda,[∥] Philippe Sautet,[∥] and Françoise Delbecq[∥]

[†]Institut Charles Gerhardt Montpellier, UMR 5253 CNRS-UM2-ENSCM-UM1, Matériaux Avancés pour la Catalyse et la Santé (MACS), Ecole Nationale Supérieure de Chimie, 8 rue de l'Ecole Normale, F-34296 Montpellier Cedex 5, France

[‡]Sorbonne Universités, UPMC Univ Paris 06, UMR 7197, Laboratoire de Réactivité de Surface, F-75005 Paris, France

[§]CNRS-UMR 7197, Laboratoire de Réactivité de Surface, F-75005 Paris, France

[∥]Université de Lyon, CNRS-Laboratoire de Chimie UMR 5182, Ecole Normale Supérieure de Lyon, 46 Allée d'Italie, F-69364 Lyon, France

Supporting Information

ABSTRACT: This combined experimental and theoretical study aims at understanding why surface hydroxyl groups may enhance catalytic reactivity of MgO surfaces in basic catalysis, whereas hydroxyls are weakly deprotonating groups. We investigated that reactivity enhancement in the catalytic conversion of 2-methyl-but-3-yn-2-ol (MBOH). Reaction kinetics was experimentally determined on partially hydroxylated MgO: active sites were saturated with the reactant and catalyzed its conversion with an activation energy of 85 kJ·mol^{-1}. Reaction pathways were calculated over fully hydroxylated, partially hydroxylated, and dehydroxylated MgO surfaces by means of first-principles simulations. To highlight the effect of reactant coverage, we also calculated the reaction pathway on MgO precovered with MBOH molecules. The results show that the surface OH groups generated by dissociative adsorption of water induce a lowering in the activation energy barriers when they keep a bare Mg^{2+}-O^{2-} pair available in the vicinity for MBOH to adsorb and react. Interestingly, OH groups do not directly interact with MBOH converting on the surface, but they modify the basic properties of the vicinal bare Mg^{2+}-O^{2-} pair on which MBOH adsorbs and converts. A similar effect is predicted when MBOH converts on a bare Mg^{2+}-O^{2-} pair in the vicinity of a second adsorbed MBOH molecule. The beneficial effect of coadsorbates on the reactivity of active sites is analyzed by means of a thermodynamic model and an electronic structure analysis.

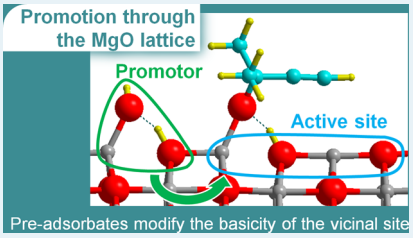

KEYWORDS: *basic catalyst, MgO, MBOH, DFT, hydroxyl, alcohol, water*

INTRODUCTION

Basic oxides play a major role as catalysts in valorization of alcohols from biomass. These materials are used in reliable after-oil processes to catalyze esterifications, transesterifications, etherifications, and even C−C bond formation through Guerbet reaction. They are intensively investigated in order to optimize their performance.[1−9] Those investigations toward applications revealed a typical behavior: strong basic sites are generally not needed for an efficient conversion of alcohols.[10−16]

Previous experimental observation is in total agreement with conclusions from fundamental studies of model reactions.[17−20] In particular, surface hydroxyls are often involved in the most active sites catalyzing alcohol conversions, even when stronger basic sites are also available on the surface. The particular role of surface hydroxyls goes beyond alcohol conversions[21,22] and appears as a key element for understanding basic catalysis: hydroxyls naturally form on all basic oxides exposed to wet atmosphere, and their formation could explain why adding water in the adducts improves other processes in basic heterogeneous catalysis.[23−28]

The catalytic role of hydroxyls was specifically proven on MgO and CaO for the conversion of a model alcohol, the 2-methylbut-3-yn-2-ol (MBOH).[19,20,29,30] The catalytic conversion of MBOH leads to the formation of different products depending on the nature of the active sites that are involved.[20] On basic oxides, MBOH conversion gives acetone and acetylene only and allows basic active sites to be revealed. In the past decade, we used that model reaction in a comprehensive multitechnique study aiming to identify active sites in basic catalysis by MgO.[29,31−33] We showed that the catalytic activity in MBOH conversion correlates with the surface concentration of hydroxyls with low coordination number (OH_{LC}).[29] The concentration of hydroxyls on MgO was measured through quantitative ^{1}H NMR analysis, which also gave insights into the coordination number of the hydroxyls involved in the active sites. However, the exact structure of the active sites could not be probed within that

Received: July 25, 2014
Revised: September 5, 2014
Published: October 10, 2014

   dx.doi.org/10.1021/cs5010807 | ACS Catal. 2014, 4, 4004−4014

study and still needs to be elucidated for understanding the mechanism.

Up to now, the catalytic role of hydroxyls was often interpreted through the Sabatier principle ("the alcohol molecule should adsorb more weakly and thus evolve more easily on hydroxylated sites than on dehydroxylated sites"), but it has never been explained at a molecular level with a specific and proven mechanism. For the most studied basic catalyst MgO, modeling studies often address interactions of protic molecules with (100) plans and defects (steps, corners, kinks),[34−41] but only few papers report full calculations of base-catalyzed reaction mechanisms.[42−45] Moreover, they always focus on bare oxide surfaces: the catalytic role of surface hydroxyls has never been addressed specifically. Interestingly, Wang et al. suggested in a recent DFT study on bare MgO that strong basic sites are not desirable for an efficient basic catalysis.[45] They calculated pathways of butene isomerization for four different models of nonhydroxylated active sites, and with their preliminary convergence criteria, the lowest activation barrier was obtained on the surface defect which was the least stabilizing for the intermediates. That study indicated that the Sabatier principle was relevant for interpreting basic catalysis, even with alkenes as reactants, which should be much harder to deprotonate than alcohols.

Beyond the Sabatier principle, it is necessary to explain why weakly deprotonating hydroxyl groups can enhance the catalytic reactivity of MgO surfaces in basic catalysis. Do the hydroxyls act as deprotonating sites or as stabilizing groups for reaction intermediates? Which structural parameters contribute to the lowering of the activation barrier?

This work aims at explaining why hydroxylated MgO surfaces catalyze basic conversion of alcohols more efficiently than bare MgO surfaces do. This explanation was brought by a modeling approach in close interaction with experiment. The present paper is organized as follows: the first section is devoted to the experimental kinetic study of MBOH conversion on hydroxylated MgO surfaces. In the second section, the conversion reaction mechanisms are exposed from density functional theory (DFT) calculations. Finally, the last section compares experimental kinetics and calculated mechanisms and proposes an interpretation of the catalytic role of surface hydroxyls in MBOH conversion from both DFT adsorption thermodynamics and local density of state analyses.

EXPERIMENTAL METHODS

Material Synthesis. MgO sample was prepared through thermal decomposition of $Mg(OH)_2$ precursor at 1273 K in vacuum. $Mg(OH)_2$ precursor was precipitated from a $Mg(NO_3)_2$ solution basified with ammonium hydroxide, as described earlier.[46] The BET specific surface area of the MgO sample was measured to be 167 $m^2 \cdot g^{-1}$.

MBOH Catalysis Experiments. MBOH reaction was followed in an automated differential flow microreactor. For each experiment, 20 mg of catalyst was pressed into wafers under a pressure of 5×10^5 Pa and crushed into pellets of 125−200 μm diameter. The sample was deposited on porous glass, in the center of a U quartz tube with a 10 mm i.d.

Just before the catalysis measurements, the catalyst surface was cleaned in situ at high temperature and partially hydroxylated as described in details earlier.[32,46] It was heated at 1023 K under dry N_2 flow, cooled to 373 K, exposed to wet N_2 flow at 373 K, and partially dehydroxylated at 673 K under dry N_2 flow. It was checked that hydroxylation treatment did not reconstruct the surface. The reaction temperature of 343−383 K was controlled within ±1 K with a thermocouple located by the catalyst. The desired MBOH partial pressure was obtained by bubbling nitrogen (100 cm^3 min^{-1}) in liquid MBOH at the selected temperature. Reaction products were analyzed every 120 s using a Varian micro gas chromatograph equipped with a catharometric detector and a CP WAX 52 CB column. It has been confirmed that by varying the mass of the sample and the inert flow rate no diffusion limitation could be observed under these conditions.

Kinetics Analysis. The partial pressure and the concentration of each product P_i was calculated from chromatographic measurements by using the appropriate response coefficients and the value of the initial partial pressure of MBOH in the feed, P^0_{MBOH}.

Acetone and acetylene are the only detected products, and they are in a ratio of 1 to 1, in agreement with the reaction equation predicted for the ideal case of purely basic MBOH conversion.

The conversion rate Conv is expressed as

$$\mathrm{Conv} = \frac{0.5 \cdot (P_{\mathrm{acetone}} + P_{\mathrm{acetylene}})}{P^0_{\mathrm{MBOH}}} \quad (1)$$

where $P_{acetone}$ and $P_{acetylene}$ are the partial pressures of acetone and acetylene, respectively.

The contact time is the ratio of the catalytic bed volume (in cm^3) to the feed flow rate (in $cm^3 \cdot s^{-1}$). Arrhenius parameters are extracted from the initial volumic rates of formation of acetone $r_f^{acetone}$ (equal to the one of acetylene). Those initial rate values are measured when the contact time approaches zero: in the graph giving the outlet concentration of acetone (in mol L^{-1}) as a function of the contact time (in s), they are given by the slope of the tangent at the origin.

THEORETICAL CALCULATIONS

Surface Model. To study the reaction mechanism at various hydroxyl coverages, we chose the edge of an MgO step. That defect can deprotonate water and alcohols, which is necessary to form surface hydroxyls[40,41] and the first reaction intermediate in alcohol conversions.[41,47] The slab (called S2ON) was used in several previous works[40,48−50] as a model of MgO surface defect involving four coordinated (4C) ions. It is one of the MgO defects that is most commonly used in theoretical study of MgO surface reactivity.[40,41,45,47−49,51−53] The model is a three-layer slab representing a 2-d_{Mg-O} high step with a 6-d_{Mg-O} long edge (where d_{Mg-O} is the Mg−O distance). It offers three sites of adsorption for water or alcohol. The two upper layers of the slab were allowed to relax during all the calculations.

First-Principles Calculations. The calculations were performed using DFT in periodic boundary conditions with the VASP program.[54,55] The general gradient approximation (GGA, Perdew−Wang 91[56,57]) was used, and the electron−ion interaction was described with the PAW method.[58] A tight convergence of the plane-wave expansion was obtained with a cutoff of 400 eV.[41] The convergence criterion for the electronic self-consistent cycle was fixed to 10^{-6} eV. Geometry optimizations were performed within a conjugate-gradient algorithm until the convergence criterion on forces (10^{-2} eV·$Å^{-1}$) was reached. In order to describe the interaction between adsorbates and the MgO surface, we defined the adsorption energy as follows:

dx.doi.org/10.1021/cs5010807 | ACS Catal. 2014, 4, 4004−4014

$$\Delta E_{ads} = E(\text{adsorbate}) - E(\text{surface}) - E(\text{gas phase}) \quad (2)$$

where E(surface), E(gas phase), and E(adsorbate) represent the energies of the optimized oxide surface (with its possible preadsorbates), gas phase reactants and adsorbed phase, respectively. E(gas phase) was calculated in periodic conditions mimicking the gas phase: one molecule in a vacuum box with 15 Å × 16 Å × 17 Å dimensions.

The transition states (TS) of the elementary steps were determined using the nudged-elastic-band (NEB) method.[59] Reaction pathways were optimized with a set of eight intermediate geometries (16 in complex cases), obtained by linear interpolation with a mixed internal and Cartesian coordinate system using the string theory,[60] as implemented in the Opt'n Path suite.[61] The obtained approximate transition states were refined by minimizing the residual forces below 10^{-2} eV·Å^{-1} with the quasi-Newton algorithm implemented in VASP. All potential energy surface (PES) extrema were verified by the calculation of the vibrational frequencies within the harmonic approximation. The Hessian or force constant matrix was computed by finite differences on nuclei forces followed by a diagonalization procedure. The resulting eigenvalues correspond to the harmonic frequencies.

Atomistic Thermodynamics. The Gibbs free energy in reaction conditions is considered with the following approach. A simple way to estimate the stability of the adsorbed species is the prediction of the Gibbs free adsorption energy ΔG_{ads} (see ref and references therein for the elaboration of the corresponding model):

$$\Delta G_{ads} = G_{ads} - G_{surf} - G_{gas} \quad (3)$$

$$\Delta G_{ads}(T, P) = \Delta E_{ads} + \Delta E_{ZPE} + F_{config,ads} - Nk_BT\ln\left(\frac{Q_{ads}^{vib}(T)}{Q_{gas}^{vib}(T)Q_{gas}^{rot}(T)Q_{gas}^{trans}(T, P)}\right) \quad (4)$$

$$F_{config,ads} = -k_BT\ln Q_{config,ads} = -k_BT\ln\left(\frac{N_{site}!}{(N_{site} - N_{ads})!N_{ads}!}\right) \quad (5)$$

where ΔE_{ads} and ΔE_{ZPE} are the DFT adsorption energy and the DFT zero point energy change due to adsorption, respectively. Q^{vib}_{ads} and Q^{vib}_{gas} are the respective vibrational partition functions of the adsorbed system and the gas phase. Q^{rot}_{gas} and Q^{trans}_{gas} are the rotational and translational partition functions of the gas phase, respectively. For the calculation of vibrational partition functions, the oxide surface vibrations at the Γ point are included systematically. $F_{config,ads}$ is the configuration free energy of the adsorbed phase.

RESULTS AND DISCUSSION

1. Kinetics Study of MBOH Conversion on Hydroxylated MgO. As shown in our previous study, partially hydroxylated MgO catalyzes basic MBOH conversion better than dehydroxylated MgO does.[29,33] When dehydroxylated MgO samples are exposed to wet atmosphere and heated under N_2 flow above 673 K, they catalyze the basic conversion of MBOH in correlation with the surface density of hydroxyl group. The linear correlation between catalytic activity and low coordinated OH surface density was shown for various morphologies of MgO and for heating temperatures between 673 and 1073 K.[29]

In the present study, we determined the rate law and the associated activation barrier for MBOH conversion catalyzed by a partially hydroxylated MgO sample. From the experimental results described above, it is expected that the most efficient active sites should include one OH group or more and that their surface density rules the catalytic activity in MBOH conversion.

MBOH conversion on our MgO sample follows the basic route only. Carbon balance was achieved within a maximum deviation of 2% and, as expected, the formation rates were equal for acetone and acetylene. As a consequence, rate laws for acetone and acetylene formations are the same. For the sake of brevity, the rest of the study only presents the rate law for acetone formation.

Whatever the reaction temperature between 343 and 383 K, changing inlet reactant concentration did not change the rate of reaction. Figure 1 shows outlet acetone concentration as a function of contact time for reaction at 353 K and for inlet MBOH concentration between $3{\cdot}10^{-4}$ mol L^{-1} and $5.9{\cdot}10^{-4}$ mol L^{-1}. For similar contact times, doubling inlet MBOH concentration did not change outlet acetone concentration significantly.

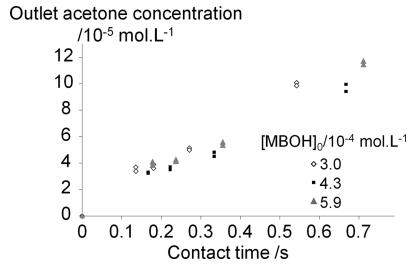

Figure 1. Kinetics of MBOH conversion at 353 K on partially hydroxylated MgO: outlet product concentration as a function of contact time for three inlet reactant concentrations $[\text{MBOH}]_0$.

As a consequence, the reaction order with respect to MBOH is zero. In initial conditions, the concentrations of acetone and acetylene are null and no other gas species contributes to the rate law. So the acetone formation obeys the following rate law:

$$r_f^{acetone} = k_{apparent}\cdot[L] \quad (6)$$

with $r_f^{acetone}$ the formation rate for acetone (in mol L^{-1}·s^{-1}), $k_{apparent}$ the apparent rate constant (in s^{-1}), and $[L]$ the active site concentration (in mol L^{-1}). That zero-order in respect to the reactant indicates that all the available active sites are saturated with adsorbed reactant.[63] That is to say, MBOH adsorbs on the active sites with a quite large energy of adsorption.

The experimental activation energy was determined from two major assumptions. First, the apparent rate constant obeys the Arrhenius equation. Second, the concentration of active sites does not change when reaction temperature varies between 343 and 383 K. Within those assumptions the logarithm of the initial rate of acetone formation $r_f^{acetone}$ is an affine function of the reciprocal reaction temperature $1/T$:

$$\ln r_f^{acetone} = \ln(k_{apparent}\cdot[L]) = -\frac{E_a}{R \times T} + \ln(A\cdot[L]) \quad (7)$$

dx.doi.org/10.1021/cs5010807 | ACS Catal. 2014, 4, 4004−4014

with the following parameters: E_a the activation energy (in J·mol^{-1}), R the universal gas constant (in J·mol^{-1}·K^{-1}), A the Arrhenius pre-exponential factor (in s^{-1}), and $[L]$ the active site concentration (in mol L^{-1}).

Fitting experimental data with eq 7 gives E_a = 85 kJ·mol^{-1} (Figure 2). With our assumptions, all the parameters of eq 7 are constant.

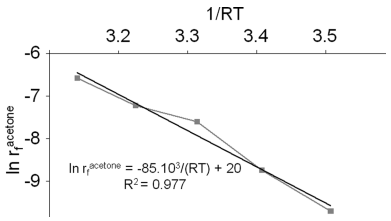

Figure 2. Kinetics of MBOH conversion at 343−383 K on partially hydroxylated MgO: Arrhenius plot from initial rates of acetone formation.

As usual with multisite catalysts, the rate law only gives an average description of the various active sites available on the MgO surface. All the surface sites of partially hydroxylated MgO do not convert MBOH with the same efficiency. Each type of active site contributes to the apparent rate constant proportionately to its own rate constant weighted by its relative concentration. Only the rate constant of one type of actives site has a chemical meaning at the molecular level. Those site-specific rate constants cannot be individually measured through our kinetics experiments, but they can be evaluated through theoretical modeling of the reaction path on each type of active sites.

2. DFT Reaction Pathways for MBOH Conversion. In spite of its high interest as a model reaction on basic oxide, the conversion of MBOH on MgO surfaces has never been studied from first-principles calculations. In this paper, we investigated the reaction mechanism at a molecular level to understand why partially hydroxylated MgO surfaces convert MBOH better than dehydroxylated surfaces do. Therefore, we calculated and compared minimum energy reaction pathways on a bare MgO step and on the same defect precovered with dissociated water molecules. In addition, in order to highlight the effect of surface coadsorption, we investigated the conversion of MBOH on MgO precovered by a second MBOH molecule.

Reaction Pathway over Dehydroxylated MgO. On an MgO stepped surface, the strongest sites for adsorption of water and alcohols are the $Mg^{2+}O^{2-}$ pairs located on the edge of the step.[40,41] The conversion reaction over dehydroxylated MgO step was modeled by considering one isolated MBOH molecule. Figure 3 gives the identified elementary steps including the intermediates and the transition states, TSs. Initially, MBOH adsorbs on an Mg^{2+}-O^{2-} pair along the edge of the step (intermediate 1) by its hydroxyl moiety and dissociates spontaneously (no accessible transition state and no activation energy). The system is strongly stabilized by −134 kJ·mol^{-1}. This stabilization energy is similar to that obtained for water and methanol adsorptions at the MgO step (respectively: −143 kJ·mol^{-1} [40] and −129 kJ·mol^{-1} [41]). The MBO^- alcoholate is adsorbed on the Lewis acid site Mg^{2+} and the proton on the Lewis base site O^{2-}, giving a multicoordinated surface hydroxyl where hydrogen is still interacting with the anionic oxygen moiety of the adsorbed alcoholate at a distance of 1.51 Å. The dissociative adsorption of isolated MBOH molecule induces a

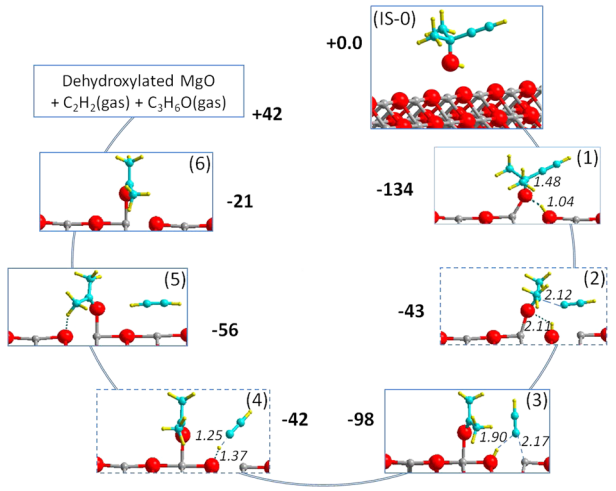

Figure 3. Atomic structures of initial (IS-0: dehydroxylated MgO edge + free MBOH), reactive (1), transition states (2, 4) and intermediates (3, 5, 6) identified along the reaction energy path of MBOH conversion to acetone and acetylene on dehydroxylated MgO surface. Reported electronic energies (in bold) are in kJ·mol^{-1} and are calculated with respect to the dehydroxylated MgO edge surface and the 1MBOH gas molecule. Indicated distances (in italic) are in Ångströms.

large relaxation of the distance between the ions of the host Mg^{2+}-O^{2-} pair (+30% in comparison with equilibrium distance without adsorbate).

The deprotonated MBOH is converted into adsorbed acetone and dissociated acetylene (intermediate 3 in Figure 3) through transition state (2). In that transition state, the reactive vibrational mode corresponds to the breaking of the C−C bond (imaginary frequency i253 cm^{-1}) and the C−C bond about to break is elongated by 0.6 Å (2.12 Å vs 1.48 Å in adsorbed MBOH intermediate). In chemical words, the MBO^- adsorbed alcoholate eliminates the acetylide leaving group, which adsorbs by its anionic end on the other Mg^{2+} ion neighboring the multicoordinated OH. Simultaneously, that OH rotates and switches the donating H interaction from MBO^- to the acetylide. To achieve this elementary step, the system should overcome a relatively high activation barrier of 91 kJ·mol^{-1}. The formed acetone and acetylide (intermediate 3) are exothermically adsorbed by −98 kJ·mol^{-1}. The acetylide intermediate is normal to the surface and interacts both with the surface hydroxyl and the Mg^{2+}_{4c} cation at distances of 1.90 and 2.17 Å, respectively.

The third step corresponds to the protonation of the adsorbed acetylide by the surface hydroxyl group (transition state 4) and the formation of adsorbed acetylene (intermediate 5). That elementary step is a Brønsted acid−base reaction. It is endothermic by 42 kJ·mol^{-1} and occurs after overcoming a barrier of 56 kJ·mol^{-1}. In the transition state, the acetylide comes close to the proton of the surface hydroxyl ($d_{C\cdots H}$ = 1.25 Å) and the angle between the acetylide and the MgO edge is 45°, halfway between the initial position perpendicular to the edge and the final, parallel. In intermediate 5, acetylene is stabilized parallel to the edge via $\pi \rightarrow Mg^{2+}$ donation and via two donor H-bonds with O^{2-}, which cause the bending of the molecule toward the surface. In the same time, acetone undergoes a rotation of more than 140°, which allows the α-hydrogen of acetone to interact with surface O^{2-}. The

dx.doi.org/10.1021/cs5010807 | ACS Catal. 2014, 4, 4004−4014

vibrational mode associated with the C−H bond formation is i372 cm^{-1}.

In the last two steps, acetylene and acetone desorb with desorption energies of 35 $kJ·mol^{-1}$ and 63 $kJ·mol^{-1}$, respectively. The Mg^{2+}-O^{2-} active site is then regenerated.

Reaction Pathway over Hydroxylated MgO. In order to investigate the effect of surface hydroxyls on the conversion of MBOH, we considered two MgO hydroxylated surfaces: the fully hydroxylated edge and the partially hydroxylated one.

Fully Hydroxylated MgO. Over the fully hydroxylated MgO edge, three water molecules are dissociatively adsorbed on the edge of the MgO diatomic step ($\theta_{(H2O)}$ = 1 ML). As the edge Mg^{2+}-O^{-} pairs are blocked by adsorbed dissociated water molecules, no strongly basic site is available on the surface.

MBOH molecularly adsorbs above the hydroxyl row by its hydroxyl moiety without dissociation. Adsorbed MBOH (intermediate 7, Figure 4) is stabilized by a complex network

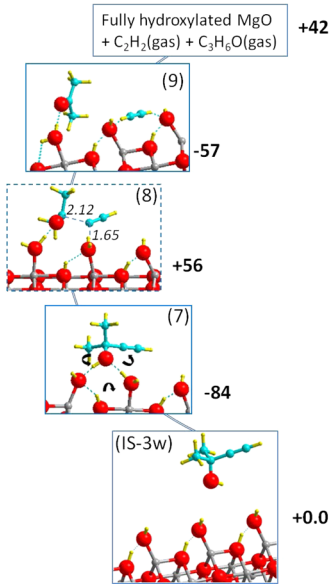

Figure 4. Atomic structure of initial (IS-3w: fully hydroxylated MgO edge + free MBOH), reactive (7), transition state (8), and intermediate (9) identified along the reaction energy path of MBOH conversion on fully hydroxylated MgO surface. Reported electronic energies (in bold) are in $kJ·mol^{-1}$ and are calculated with respect to the fully hydroxylated MgO edge surface and 1MBOH gas. Indicated distances (in italic) are in Ångströms. For simplification, the intermediate (10) corresponding to adsorbed acetone was omitted.

of H bonds with the surface hydroxyls. On that system, the adsorption energy is predicted to be of −84 $kJ·mol^{-1}$, which is 50 $kJ·mol^{-1}$ less intense than on the dehydroxylated surface.

According to our calculations, molecularly adsorbed MBOH converts into adsorbed acetone and acetylene in a concerted manner (intermediate 9). No alcoholate or acetylide intermediate was isolated in our calculations. The predicted activation energy barrier of 140 $kJ·mol^{-1}$ is higher by 49 $kJ·mol^{-1}$ than the identified one on dehydroxylated MgO. The identified transition state (TS 8) corresponds to a six-membered ring surface species. During the C−C bond breaking, some protons jump through H-bonds and the network of H-bonds is continuously modified: (i) the acetylide leaving group catches the proton of a donor hydroxyl, (ii) the alcohol gives its proton to the surface acceptor hydroxyl through the H-bond existing in the initial intermediate, (iii) the formed acetylene rotates to interact with two surface acceptor hydroxyls, (iv) acetone interacts with the donor hydroxyl of the water molecule. In the transition state, the length of the C−C bond about to break is the same as the one in the C−C breaking TS on dehydroxylated MgO surface (2.12 Å). The computed imaginary vibrational mode is i285 cm^{-1}.

Over the fully hydroxylated MgO surface, the adsorbed acetone and acetylene intermediates are stabilized with similar energy (−57 $kJ·mol^{-1}$) to that found on bare MgO. These produced molecules desorb with calculated energies of 40 and 60 $kJ·mol^{-1}$, respectively.

Partially Hydroxylated MgO. The partial hydroxylation of the oxide surface was obtained through dissociative adsorption of one water molecule ($\theta_{(H2O)}$ = 1/3 ML), giving two H-bonded hydroxyls: one monocoordinated adsorbed on an edge Mg^{2+} and one multicoordinated obtained by protonation of an edge O^{2-}. Thus, the partially hydroxylated oxide surface offers three adsorption sites for the coming MBOH gas molecule:

(i) Mg^{2+}-O^{2-} pair next to the monocoordinated hydroxyl. When MBOH adsorbs here, it interacts with that hydroxyl via its ethynyl moiety, which induces the reformation of the water molecule (Figure 5, intermediate 11).

ii) Mg^{2+}-O^{2-} pair next to the multicoordinated hydroxyl (Figure 6, intermediate 15). In this configuration, the water molecule remains dissociated.

(iii) Over the hydroxyls of the dissociated water molecule. In this case, MBOH interacts with the surface only through hydrogen bonds with those hydroxyls. This adsorption configuration of MBOH is not considered in the rest of the study because it is less stable than the two first configurations (−91 $kJ·mol^{-1}$ for both), and in all our optimization attempts, it naturally evolved into configurations with MBOH dissociated on a free Mg^{2+}-O^{2-} pair.

From the two selected configurations for adsorbed MBOH, we identified two possible routes for the conversion reaction. In the first route (Figure 5), the surface water molecule participates into the reaction ("actor surface hydroxyl"). In the second route (Figure 6), the dissociated water molecule remains spectator ("spectator surface hydroxyl") during the conversion reaction.

Actor Hydroxyl. On the partially hydroxylated surface, MBOH dissociatively adsorbs with an exothermicity of −91 $kJ·mol^{-1}$ (intermediate 11). This adsorption is 42 $kJ·mol^{-1}$ weaker than the one on the dehydroxylated step and 7 $kJ·mol^{-1}$ stronger than the one on the fully hydroxylated edge. Similarly to the case of the fully hydroxylated edge, MBOH directly converts into acetone and acetylene (intermediate 13). That concerted reaction involves a complex process of proton transfers and implies to overcome a high activation energy barrier of 129 $kJ·mol^{-1}$. At the transition state (TS (12)), the ethynyl moiety comes closer to the proton of the water hydroxyl (from 2.40 to 1.55 Å) and three concerted processes occur: (i) the C−C bond is breaking (2.35 Å in TS (12) vs 2.12 Å in TS (2)), (ii) the acetylide catches the proton, and (iii) the surface multicoordinated hydroxyl rotates and the H-bond shifts from the about-to-form acetone to the surface monocoordinated acceptor hydroxyl resulting from water deprotonation. The imaginary frequency related to the C−C bond breaking is i257 cm^{-1}. The final intermediate with acetone adsorbed on an edge Mg^{2+} and acetylene interacting

dx.doi.org/10.1021/cs5010807 | ACS Catal. 2014, 4, 4004−4014

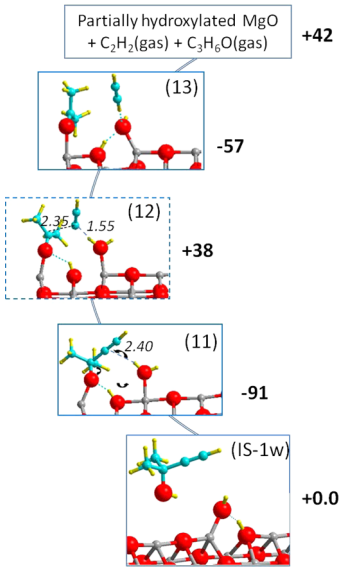

Figure 5. Atomic structure of initial (IS-1w: partially hydroxylated MgO edge + free MBOH), reactive (11), transition state (12), and intermediate (13) identified along the reaction energy path of MBOH conversion with preadsorbed water molecule involved in the reaction process (actor hydroxyl). Reported electronic energies (in bold) are in kJ·mol^{-1} and are calculated with respect to the MgO edge surface with preadsorbed H_2O and 1MBOH gas. Indicated distances (in italic) are in Å. For simplification, the intermediate (14) corresponding to adsorbed acetone was omitted.

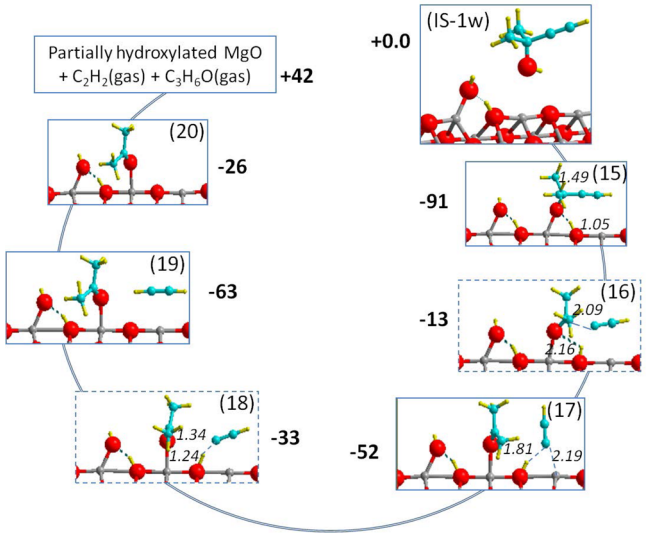

Figure 6. Atomic structure of initial (IS-1w: partially hydroxylated MgO edge + free MBOH), reactive (15), transition states (16, 18), intermediates (17, 19, 20) identified along the reaction energy path of MBOH conversion with preadsorbed water molecule non involved in the reaction process (spectator hydroxyl). Reported electronic energies (in bold) are in kJ·mol^{-1} and are calculated with respect to the MgO edge surface with preadsorbed H_2O and MBOH gas. Indicated distances (in italic) are in Å.

with one surface hydroxyl (intermediate 13) is stabilized by −57 kJ·mol^{-1}. This value is the same as the one obtained in the cases of the fully hydroxylated and of the dehydroxylated MgO surface. Finally, adsorbed acetylene desorbs with desorption energy of 34 kJ·mol^{-1}, acetone desorbs with desorption energy of 65 kJ·mol^{-1}, and the active site is regenerated.

Spectator Hydroxyl. In the case of spectator hydroxyl, the Mg^{2+}-O^{2-} pair at the side of ethynyl moiety of the adsorbed MBOH is free. Therefore, as in the case of dehydroxylated MgO, the conversion of dissociated MBOH to acetone and acetylene occurs by the intermediary formation of an adsorbed acetylide. The resulting intermediate 17 with adsorbed acetone and acetylide is geometrically quasi-identical to the intermediate 3 (Figure 3), generated over dehydroxylated MgO. However, the activation energy (78 kJ·mol^{-1}) is 13 kJ·mol^{-1} lower than the calculated barrier on the dehydroxylated surface. In the transition state, the C−C bond about to break is 2.09 Å long and the associated imaginary frequency is i252 cm^{-1}. In the same way, the stabilization energies of the intermediates are smaller in the presence of the spectator hydroxyls than in their absence: adsorbed MBOH and the resulting coadsorbed acetone and acetylide are stabilized more weakly on this partially hydroxylated edge (respectively −91 and −52 kJ·mol^{-1}) than on the dehydroxylated one (respectively −134 and −98 kJ·mol^{-1}). In the third step, the acetylide catches the proton of the multicoordinated surface hydroxyl with which it interacts in intermediate 17 and forms acetylene adsorbed close to acetone (intermediate 19). This Brønsted acid−base elementary reaction step is exothermic (−11 kJ·mol^{-1}) and occurs after overcoming a small barrier of 19 kJ·mol^{-1} (TS 18). Finally, similarly to the previously described paths, acetylene and acetone can desorb alternatively.

From the theoretical exploration of the reaction pathways, it appears that the presence of a spectator hydroxyl group on the MgO edge lowers the activation barriers of MBOH conversion with respect to the dehydroxylated edge. This result may explain why the catalytic activity of the MgO surface is experimentally enhanced by surface hydroxylation.

That important modeling result also raises the question of the surface environment effect on the surface oxide basicity. Preadsorbed hydroxyls influence the basic reactivity of the surface but they directly interact neither with adsorbed MBOH nor with the successive species during the conversion mechanism. So, from our calculations, the influence is not directly linked to the particular properties of the hydroxyl adsorbates (e.g., their ability to donate H-bond) and it could be observed with other preadsorbates. In the following, we address the question of how other spectator preadsorbates could influence the reactivity. Because our experimental study provides evidence for a large coverage of active sites with MBOH, we present the modeled reaction pathway of MBOH conversion in the presence of preadsorbed MBOH.

Reaction Pathway in the Presence of Coadsorbed MBOH. On the MgO edge with one preadsorbed MBOH molecule (coverage of the edge 1/3 ML), the MBOH reactant adsorbs dissociatively with an adsorption energy (−90 kJ·mol^{-1}) similar to that calculated in the presence of one neighboring water molecule (−91 kJ·mol^{-1}). During this coadsorption process (intermediate 21, Figure 7) the MBOH coverage is equal to 2/3 ML. Regardless of the starting structural configuration, the geometry optimization leads to two adjacent MBO^- adsorbates oriented in two quasi-perpendicular directions. This orientation mismatch may arise from steric hindrance between methyl and ethynyl moieties of the two adsorbates. The converted MBOH is the one in which the ethynyl moiety is coplanar with the proton adsorbed on the edge.

Similarly to the case of partially hydroxylated surface with a spectator hydroxyl, the deprotonated MBOH is first converted

dx.doi.org/10.1021/cs5010807 | ACS Catal. 2014, 4, 4004−4014

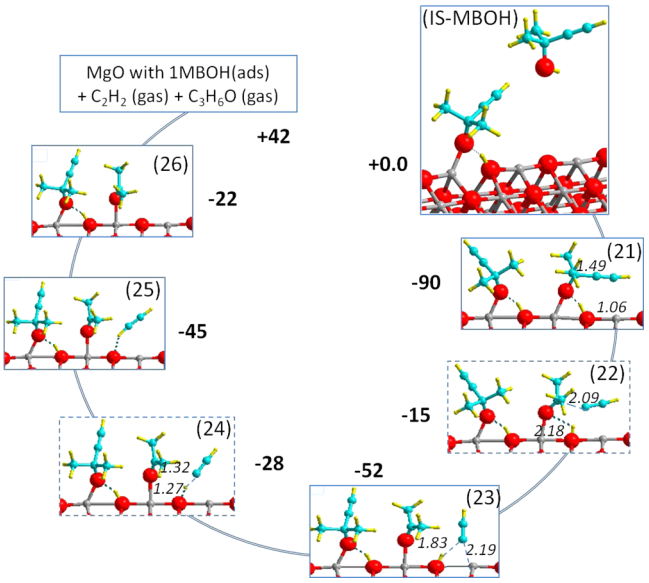

Figure 7. Atomic structure of initial (IS-MBOH: MgO edge with one adsorbed MBOH molecule + free MBOH), reactive (21), transition states (22, 24), and intermediates (23, 25, 26) identified along the reaction energy path of MBOH conversion with preadsorbed MBOH. Reported energies (in bold) are in kJ·mol^{-1} and are calculated with respect to the MgO edge surface with preadsorbed MBOH and 1MBOH gas. Indicated distances (in italic) are in Å.

into adsorbed acetone and acetylide (intermediate 23, Figure 7) through a relatively small activation barrier of 75 kJ·mol^{-1}. In the same way, this step is reached after the elongation of the about-to-break C−C bond from 1.49 to 2.09 Å in TS 22. The corresponding imaginary frequency is i249 cm^{-1}.

The further steps are similar to those identified on the partially hydroxylated surface with spectator hydroxyl, except a slight difference on the computed energy of the products. Indeed, intermediate 25 with adsorbed acetone and acetylene is less stabilized than the analogous intermediate 19 by about 18 kJ·mol^{-1}. That difference comes from the different modes of coordination of acetylene in the two intermediates: in intermediate 25, the molecule is only stabilized by one donor H-bond with a surface O^{2-} whereas in intermediate 19, acetylene interacts with the surface through two donor H-bonds with O^{2-} and one donor π interaction with Mg^{2+}.

3. DISCUSSION

After having explored in details the DFT reaction pathways of the MBOH conversion on the MgO stepped surface, in several conditions of hydration and MBOH coverage, we compare those pathways to propose an interpretation of the experimental kinetics measurements.

For all the mechanisms with preadsorbed molecules, the rate-determining step is the C−C bond breaking. That step has the highest transition state. In the case of dehydroxylated surfaces, the TSs for the C−C breaking and the protonation of acetylide show a similar energy. For clarity, we have retained the activation barriers of the C−C bond breaking step as the key theoretical element to compare the kinetic contributions of all the mechanisms and interpret the kinetic measurements.

In the two mechanisms in which surface hydroxyls directly interact with MBOH (on fully hydroxylated edge and on partially hydroxylated edge), the activation barriers (140 and 129 kJ·mol^{-1}) are much larger than those of all the other cases and the TSs of the C−C bond breaking are even higher than the initial states with the MBOH in the gas phase. That means that those mechanisms with actor hydroxyls are very unlikely to happen experimentally, because in those cases, MBOH would desorb rather than convert. Those mechanisms are not discussed further.

Figure 8 shows the energy profiles of the three retained competitive mechanisms, in which MBOH converts in three

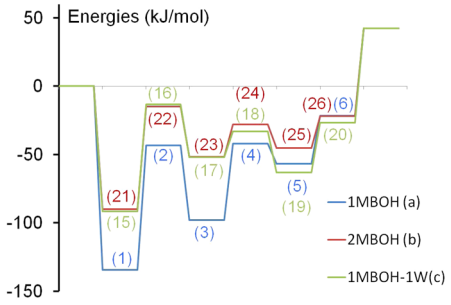

Figure 8. Energy profiles of competitive MBOH conversion reaction pathways. Relative electronic energies are calculated with respect to the (a) clean MgO edge surface and one MBOH gas molecule; (b) MgO edge surface with one adsorbed MBOH molecule and one MBOH gas molecule; (c) MgO edge surface with one adsorbed water molecule (W) and one MBOH gas molecule.

different environments: (a) on the dehydroxylated MgO surface, (b) in the presence of a spectator hydroxyl species, and (c) in the presence of a preadsorbed MBOH molecule. The profiles report total electronic energies. The reaction is globally endothermic (42 kJ·mol^{-1} at 0 K), but exergonic (with a reaction free energy of −45 kJ·mol^{-1} at 400 K, comparable with 52 kJ·mol^{-1} from thermodynamic data). The entropic contribution is −217 J·mol^{-1}·K^{-1} at 400 K, one MBOH molecule giving two product molecules.

The calculated activation barriers of the rate-determining step for the three competitive pathways ($\Delta E_{act,eff}$ = 91, 75, 78 kJ·mol^{-1}) are close to the experimental apparent activation energy (85 kJ·mol^{-1}). Such a consistency also confirms that with the MgO edge, we model pathways whose energetics is relevant to understand MgO basic reactivity.

The DFT results predict that MBOH conversion would be easier and faster on surfaces precovered with adsorbed H_2O or MBOH molecules than on dehydroxylated surfaces. Precovered surface exhibit activation barriers for the rate-determining step in MBOH conversion (75−78 kJ·mol^{-1}) lower than dehydroxylated surface (91 kJ·mol^{-1}). The lowering of the activation barrier appears when the precursor state is destabilized (−90 kJ·mol^{-1} for the intermediates 15 and 21 with the preadsorbed molecules to be compared with −134 kJ·mol^{-1} for the intermediate 1 without preadsorbate). When H_2O or MBOH is preadsorbed next to a free and available Mg^{2+}-O^{2-} pair, the about-to-react MBOH molecule dissociates on that pair but adsorbs less tightly, which makes it more reactive in the rate-determining step.

The DFT calculations also bring interesting insights on the coverage of the active sites. Indeed, stabilization of the reactant on the active site decreases in the presence of coadsorbates, but the calculated adsorption energies of MBOH with coadsorbates (−90 kJ·mol^{-1} for intermediates 15 and 21) remain large enough to induce a high coverage at the experimental reaction temperature (343−383 K). In fact, when free coadsorption

dx.doi.org/10.1021/cs5010807 | ACS Catal. 2014, 4, 4004−4014

energy is considered for the adsorption of several MBOH molecules, following the same approach, the thermodynamic analysis shows that 2MBOH coadsorption is favored over 1MBOH adsorption up to 430 K. That predicted high coverage is consistent with the experimental kinetic measurements showing that the active sites on hydroxylated MgO are saturated with the reactant. In other words, preadsorbed water can tune the energy barriers without overturning the mechanism nor jeopardizing the reactant coverage.

Another important issue concerns the stability of the promotor (preadsorbed water or MBOH) during the catalytic MBOH conversion. Theoretically indeed, desorption of the promotor could directly affect the catalytic activity and the catalyst lifetime because, numerically, heat of MBOH adsorption would be enough to reassociate and desorb water or MBOH. Experimentally, however, water desorption is not observed. With hydroxylated MgO, the catalytic activity remains stable and higher than with dehydroxylated MgO. It suggests that the adsorption of water and MBOH are irreversible in the reaction conditions.

In summary, from the electronic energies, preadsorbed water and MBOH have the same promoting effect on the catalytic MBOH conversion. To discriminate the competitive reaction pathways with preadsorbed water and MBOH molecules, we revisited that analysis by considering the entropic contributions to the activation barrier of the C−C breaking step with Gibbs energy calculations.

According to (eq 4), the Gibbs free activation energy can be expressed as the sum of the activation barrier given by total electronic energy calculations ($\Delta E_{act,eff}$), the change of zero point energy between the adsorbed initial state (IS) and the TS (ΔE_{ZPE}), and the change of the vibrational entropic contribution to the Gibbs free energy (ΔG_{vib}) calculated at 400 K, again between the IS and the TS:

$$\Delta G_{act,eff}(T) = \Delta E_{act,eff} + \Delta E_{ZPE} + \Delta G_{vib}(T) \quad (8)$$

As shown in Table 1, the Gibbs effective activation energies of the first step of the reaction mechanism are 87, 70, and 71 kJ·mol^{-1}, respectively, for the dehydroxylated surface, the partially hydroxylated surface and the MBOH-precovered surface. As observed from the total electronic energy results, the Gibbs effective activation barriers evaluated for the preadsorbed cases are similar (70−71 kJ·mol^{-1}). The barriers are, however, lower than in the dehydroxylated case (of about 17−18 kJ·mol^{-1}). Hence, the relative height of the activation barriers for the two precovered surfaces is not significantly modified by adding entropy and ZPE contributions. This weak modification is explained with the indirect role of the preadsorbates in the mechanism: because they are "spectator" surface species in the reaction pathways, they do not interact directly with the moieties of the reacting MBOH, so their vibrational properties are weakly modified during the reaction.

Table 1. Energetics of the C−C Bond-Breaking Elementary Step for MBOH Conversion on the MgO Step without Pre-Adsorbate, with Pre-Adsorbed Water, and with Pre-Adsorbed MBOH

T = 400 K	ΔE_{reac}	ΔG_{reac}	$\Delta E_{act.eff}$	$\Delta G_{act.eff}$	ΔE_{ZPE}	ΔG_{vib}	freq
TS (2)	36	21	91	87	−5	2	253
TS (16)	39	23	78	70	−6	−2	252
TS (22)	38	18	75	71	−5	1	249

Total electronic energies (ΔE_{reac}) and Gibbs energies (ΔG_{reac}) of reaction correspond to the elementary step converting adsorbed MBOH into adsorbed acetone and adsorbed dissociated acetylene. The effective activation Gibbs energies ($\Delta G_{act.eff}$) of the same elementary step is decomposed as the sum of DFT effective activation energies ($\Delta E_{act.eff}$), zero-point energy changes (ΔE_{ZPE}), and change of vibrational entropic contributions of the Gibbs free energies computed at 400 K (ΔG_{vib}), between the IS and the TS. Those values (kJ·mol^{-1}) are reported for the three competitive reaction pathways identified by the Transitions State on which the C−C bond breaking occurs: TS(2) on dehydroxylated surface, TS(16) in the presence of spectator hydroxyl, TS(22) in the presence of preadsorbed MBOH. The imaginary frequencies (freq) are also addressed (cm^{-1}).

The beneficial effect of these preadsorbed molecules seems to originate from a modification of the properties of the neighboring Mg^{2+}-O^{2-} pair on which MBOH adsorbs before converting. The two considered preadsorbates have different structures and sizes (H_2O is small, whereas MBOH is quite bulky) but they exhibit the same influence on the adsorption energies and the activation barriers. The simplest explanation for the invariance toward the preadsorbate structure is that the preadsorbates influence the properties of the reacting MBOH molecule indirectly, via the oxide surface. To determine the nature of that influence, we considered two parameters: the electronic properties of the neighboring Mg^{2+}-O^{2-} pair and the geometric relaxation of the surface ions with adsorbates. For the sake of clarity, we limit the discussion to the adsorption properties toward the reacting MBOH, because we have seen that the activation barrier of the C−C bond-breaking step mainly depends on the stability of the initial state.

On the one hand, the presence of preadsorbates alters the electronic properties of the vicinal free Mg^{2+}-O^{2-} pairs by weakening the Lewis basicity of the O^{2-} ion. For the three models (bare edge, edge with one preadsorbed water molecule, edge with preadsorbed MBOH), we analyzed the projected local density of states (LDOS, Figure S1 in Supporting Information) for the surface oxide ion that catches the proton of the dissociated MBOH in the first step of the mechanism. The 2s and $2p_Z$ orbitals of that surface oxygen are affected by the presence of the preadsorbed molecule in similar ways. Over precovered MgO (with adsorbed H_2O or MBOH molecule), the surface oxygen of the Mg^{2+}-O^{2-} pair on which MBOH adsorbs before converting has a Lewis base character lower than on the reference dehydroxylated surface (the orbitals are shifted away from the Fermi level). As a consequence, the proton from MBOH is less strongly adsorbed on the surface (O−H distance is 1.04 Å for precursor 1 (Figure 3) and 1.05−1.06 Å for precursors 15 and 21 (Figures 6,7), respectively). This result can explain why MBOH adsorbs more tightly (by −44 kJ·mol^{-1}) on a dehydroxylated step than on a step precovered with water or MBOH and why the adsorbed proton is less reactive with respect to acetylide. To summarize, the MgO surface plays an important role in deprotonating the MBOH molecule but the MBO^- alcoholate eliminates its acetylide leaving group only when the dissociated H^+ is not engaged in an excessively strong basic interaction with the surface.

On the other hand, the presence of preadsorbates clearly hinders the relaxation of the surface during the subsequent adsorption of the reacting MBOH. On a bare step, when MBOH adsorbs, the surface strongly relaxes (cf. intermediate 1): the ions Mg^{2+} and O^{2-} of the adsorbing pair move apart and the Mg^{2+}-O^{2-} distance increases by 30% in comparison with bulk equilibrium distance, which allows an efficient H-bond to form between the multicoordinated hydroxyl and the oxygen of

dx.doi.org/10.1021/cs5010807 | ACS Catal. 2014, 4, 4004−4014

the alcoholate. The local stretching of the adsorbing Mg^{2+}-O^{2-} pair is absorbed by the surface framework, resulting in a lateral contraction (−6%) of the two neighboring free Mg^{2+}-O^{2-} pairs on the edge. The same phenomenon is predicted for the adsorption of one water molecule on the bare edge (Mg^{2+}-O^{2-} distances: +30% for the adsorbing pair, −6% for the neighboring pairs). Hence, when a supplementary MBOH molecule adsorbs in the vicinity of the preadsorbed molecule, it arrives on a contracted free Mg^{2+}-O^{2-} pair and needs to adapt its adsorption structure. There is a balance between the optimization of the H-bonds and the antagonist relaxation of the two adsorbing Mg^{2+}-O^{2-} pairs (Mg^{2+}-O^{2-} distances: + 17% for the pair adsorbing the spectator molecule, + 9−11% for the pair adsorbing the reacting MBOH). This compromise justifies the loss of stability registered for the second adsorbate and the resulting increase of reactivity. That phenomenon of hindered relaxation also explains why the other coadsorbed intermediates (acetone and acetylide) are not so much stabilized in the presence of preadsorbed molecule on the neighboring pair.

The promoting effect of partial hydroxylation has been evidenced and explained in our calculations, but the study prompts an open question: experimentally, why does dehydroxylated MgO convert MBOH at high coverage not so efficiently than hydroxylated MgO does? That question would require a whole study including molecular dynamics of MBOH adsorption but we may propose one explanation. The coverage state used in our modeling at "high MBOH coverage" is quite specific because the promotion by coadsorption of MBOH requires two conditions: (i) the two MBOH molecules should adsorb on vicinal Mg^{2+}-O^{2-} pairs and (ii) a third free Mg^{2+}-O^{2-} pair should be available in the vicinity of the reacting MBOH molecule to stabilize the acetylide leaving group. With the bulky structure of the MBOH molecule, the probability of vicinal coadsorption of MBOH with other free Mg^{2+}-O^{2-} pairs around could be experimentally limited. In comparison, the partially hydroxylated surface would offer promoted sites more available for MBOH adsorption. Morevover the promotion by hydroxylation would be even better when the hydroxylation of the catalyst goes beyond surface functionalization and reconstructs (100) planes into hydroxylated steps or defects.[49,50,64,65]

This work allows us to revisit the mechanisms proposed for the promotion effect of surface hydroxylation in MBOH conversion by MgO. Chizallet et al[29] proposed several mechanism hypotheses to explain the experimental correlation between the MBOH conversion rate and density of low-coordinated MgO hydroxyls. In their preferred hypotheses, MBOH adsorbs and reacts directly on OH groups via consecutive or concerted reactions. Those mechanisms may be modeled with our calculated pathways "fully hydroxylated edge" or "actor hydroxyls on partially hydroxylated edge". From our calculations, that direct involvement of OH groups appears very unlikely because the high activation barriers for the C−C bond breaking would largely favor the desorption of the reactant. On the reverse, we show that OH groups preadsorbed on a low-coordinated Mg^{2+}-O^{2-} pair may promote the conversion of MBOH on a free Mg^{2+}-O^{2-} pair in immediate vicinity of those OHs. In that case, the OH groups are spectator in the mechanism: they destabilize intermediates and lower activation barriers by hindering the relaxation of the active site and by modifying their intrinsic acido-basic properties.

From this study, a proposition of active site for hydroxylated MgO would be a free Mg^{2+}-O^{2-} pair in immediate vicinity of preadsorbed hydroxyls. Chizallet et al. excluded that type of site and the related mechanism because it would generate a maximum in the evolution of MBOH conversion rate as a function of the density of low-coordinated MgO hydroxyls.[29] Because our work excludes MBOH conversion catalyzed by hydroxyls only, it suggests that this maximum in conversion rate should exist but has not been evidenced yet. For example, such a maximum has been evidenced on CaO, which is a alkaline-earth oxide with the same structure as MgO.[30] The previous experimental work on MgO might have not explore temperature ranges for which the MgO surface is saturated with OH groups, keeping the decrease of conversion rate out of sight.

CONCLUSION

Experimentally hydroxylated MgO surfaces are found to catalyze basic conversion of MBOH better than dehydroxylated MgO surfaces do. That observation was interpreted in the literature through different hypotheses, including a concerted mechanism in which MBOH converts into acetone and acetylene in one step, thanks to the assistance of surface hydroxyl groups. With the DFT calculations performed on a stepped MgO surface and exposed in this article, we show that the concerted mechanism is very unlikely and that the surface OH groups generated by dissociative adsorption of water do not act directly as single active sites. We propose as active site a free Mg^{2+}-O^{2-} pair neighboring a preadsorbed dissociated water molecule and another free Mg^{2+}-O^{2-} pair. The neighboring hydroxyls modify the basic properties of the Mg^{2+}-O^{2-} pair on which MBOH adsorbs before converting, and the other free Mg^{2+}-O^{2-} pair next to the adsorption site stabilizes the adsorbed acetylide anion generated in the mechanism. From our calculations, however, preadsorbed MBOH has a similar beneficial influence on the catalytic activity of the Mg^{2+}-O^{2-} pairs in its vicinity, at the condition that the active site exhibits the same configuration as described just above. The experiment suggests that such a specific configuration of active site can be reached with preadsorption of water but not with direct reaction of MBOH at high coverage.

This combined experimental and theoretical work addresses for the first time in the mechanisms of basic heterogeneous catalysis the role of the hydroxyls and the relationship between adsorption strength and activation energy at the molecular scale. It opens interesting perspectives for the design of basic catalysts: the conversion of alcohols seems favored by active sites with moderate basic strength and the appropriate strength could be obtained with surface functionalization.

ASSOCIATED CONTENT

Supporting Information

Projected local density of states for the MgO surface O^{2-} ion deprotonating MBOH for the three competitive pathways. This material is available free of charge via the Internet at http://pubs.acs.org.

AUTHOR INFORMATION

Corresponding Authors

*E-mail: hugo.petitjean@enscm.fr.
*E-mail: hazar.guesmi@enscm.fr.

Notes

The authors declare no competing financial interest.

■ ACKNOWLEDGMENTS

This work was granted access to the HPC resources of (CCRT/CINES/IDRIS) under the allocation 2010 (x2010081847) made by GENCI (Grand Equipement National de Calcul Intensif). H.P. gratefully thanks Prof. R. Schloegl (Fritz Haber Institute of the Max Planck Society, Berlin, and Max Planck Institute for Chemical Energy Conversion, Mülheim an der Ruhr, Germany) for stimulating discussions on MgO reactivity.

■ REFERENCES

(1) Ménétrey, M.; Markovits, A.; Minot, C.; Pacchioni, G. *J. Phys. Chem. B* **2004**, *108*, 12858−12864.
(2) Goniakowski, J.; Noguera, C.; Giordano, L.; Pacchioni, G. *Phys. Rev. B* **2009**, *80* (12), 125403/1−125403/7.
(3) Ugliengo, P.; Damin, A. *Chem. Phys. Lett.* **2002**, *366* (5,6), 683−690.
(4) Calatayud, M.; Markovits, A.; Menetrey, M.; Mguig, B.; Minot, C. *Catal. Today* **2003**, *85*, 125−143.
(5) Calatayud, M.; Markovits, A.; Minot, C. *Catal. Today* **2004**, *89*, 269−278.
(6) Birky, T. W.; Kozlowski, J. T.; Davis, R. J. *J. Catal.* **2013**, *298*, 130−137.
(7) Kozlowski, J. T.; Behrens, M.; Schloegl, R. *Chem. Catal. Chem.* **2013**, *5* (7), 1989−1997.
(8) Di Cosimo, J. I.; Apesteguía, C. R.; Ginés, M. J. L.; Iglesia, E. *J. Catal.* **2000**, *190*, 261−275.
(9) Di Cosimo, J. I.; Diez, V. K.; Xu, M.; Iglesia, E.; Apesteguia, C. R. *J. Catal.* **1998**, *178* (2), 499−510.
(10) Aramendia, M. A.; Borau, V.; Jimenez, C.; Marinas, J. M.; Romero, F. J. *J. Colloid Interface Sci.* **1999**, *217* (2), 288−298.
(11) Breuer, K.; Teles, J. H.; Demuth, D.; Hibst, H.; Schafer, A.; Brode, S.; Domgorgen, H. *Angew. Chem., Int. Ed.* **1999**, *38* (10), 1401−1405.
(12) Aramendia, M. A.; Borau, V.; Jimenez, C.; Marinas, J. M.; Romero, F. J. *Colloids Surf., A* **2000**, *170* (1), 51−58.
(13) Arzamendi, G.; Arguinarena, E.; Campo, I.; Zabala, S.; Gandia, L. M. *Catal. Today* **2008**, *133−135*, 305−313.
(14) Ochoa-Gomez, J. R.; Gomez-Jimenez-Aberasturi, O.; Maestro-Madurga, B.; Pesquera-Rodriguez, A.; Ramirez-Lopez, C.; Lorenzo-Ibarreta, L.; Torrecilla-Soria, J.; Villaran-Velasco, M. C. *Appl. Catal., A* **2009**, *366* (2), 315−324.
(15) Tsuchida, T.; Kubo, J.; Yoshioka, T.; Sakuma, S.; Takeguchi, T.; Ueda, W. *J. Catal.* **2008**, *259* (2), 183−189.
(16) Diallo-Garcia, S.; Laurencin, D.; Krafft, J. M.; Casale, S.; Smith, M. E.; Lauron-Pernot, H.; Costentin, G. *J. Phys. Chem. C* **2011**, *115*, 24317−24327.
(17) Ai, M. *J. Catal.* **1975**, *40* (3), 318−326.
(18) Lahousse, C.; Bachelier, J.; Lavalley, J. C.; Lauron-Pernot, H.; Le Govic, A. M. *J. Mol. Catal. A* **1994**, *87* (2−3), 329−332.
(19) Lauron-Pernot, H.; Luck, F.; Popa, J. M. *Appl. Catal., A* **1991**, *78*, 213−225.
(20) Lauron-Pernot, H. *Catal. Rev.* **2006**, *48*, 315−361.
(21) Wischert, R.; Copéret, C.; Delbecq, F.; Sautet, P. *Angew. Chem., Int. Ed.* **2011**, *50*, 3202−3205.
(22) Wischert, R.; Laurent, P.; Copéret, C.; Delbecq, F.; Sautet, P. *J. Am. Chem. Soc.* **2012**, *134*, 14430−14449.
(23) Zhang, G.; Hattori, H.; Tanabe, K. *Appl. Catal., A* **1988**, *36*, 189−197.
(24) Rao, K.; Gravelle, M.; Sanchez-Valente, J.; Figueras, F. *J. Catal.* **1998**, *173* (1), 115−121.
(25) Prinetto, F.; Tichit, D.; Teissier, R.; Coq, B. *Catal. Today* **2000**, *55* (1), 103−116.
(26) Wang, J. A.; Bokhimi, X.; Novaro, O.; Lopez, T.; Gomez, R. *J. Mol. Catal. A* **1999**, *145*, 291−300.
(27) Kus, S.; Otremba, M.; Torz, A.; Taniewski, M. *Fuel* **2002**, *81* (13), 1755−1760.
(28) Tielens, F.; Minot, C. *Surf. Sci.* **2006**, *600* (2), 357−365.
(29) Chizallet, C.; Petitjean, H.; Costentin, G.; Lauron-Pernot, H.; Maquet, J.; Bonhomme, C.; Che, M. *J. Catal.* **2009**, *268*, 175−179.
(30) Petitjean, H.; Krafft, J. M.; Che, M.; Lauron Pernot, H.; Costentin, G. *Phys. Chem. Chem. Phys.* **2010**, *12*, 14740−14748.
(31) Chizallet, C.; Bailly, M. L.; Costentin, G.; Lauron-Pernot, H.; Krafft, J. M.; Bazin, P.; Saussey, J.; Che, M. *Catal. Today* **2006**, *116* (2), 196−205.
(32) Bailly, M. L.; Chizallet, C.; Costentin, G.; Krafft, J. M.; Lauron-Pernot, H.; Che, M. *J. Catal.* **2005**, *235* (2), 413−422.
(33) Chizallet, C.; Costentin, G.; Lauron-Pernot, H.; Krafft, J. M.; Bazin, P.; Saussey, J.; Delbecq, F.; Sautet, P.; Che, M. *Oil Gas Sci. Technol.* **2006**, *61* (4), 479−488.
(34) Branda, M. M.; Horacio Rodriguez, A.; Belelli, P. G.; Castellani, N. J. *Surf. Sci.* **2009**, *603* (8), 1093−1098.
(35) Calatayud, M.; Ruppert, A. M.; Weckhuysen, B. M. *Chem.—Eur. J.* **2009**, *15* (41), 10864−10870.
(36) Di Valentin, C.; Vitto, A. D.; Pacchioni, G.; Abbet, S.; Wörz, A. S.; Judai, K.; Heiz, U. *J. Phys. Chem. B* **2002**, *106* (46), 11961−11969.
(37) Gay, I. D.; Harrison, N. M. *Surf. Sci.* **2005**, *591* (1−3), 13−22.
(38) Costa, D.; Chizallet, C.; Ealet, B.; Goniakowski, J.; Finocchi, F. *J. Chem. Phys.* **2006**, *125* (5), 054702/1−054702/10.
(39) Wlodarczyk, R.; Sierka, M.; Kwapien, K.; Sauer, J. *J. Phys. Chem. C* **2011**, *115* (14), 6764−6774.
(40) Chizallet, C.; Costentin, G.; Che, M.; Delbecq, F.; Sautet, P. *J. Phys. Chem. B* **2006**, *110* (32), 15878−15886.
(41) Petitjean, H.; Tarasov, K.; Delbecq, F.; Sautet, P.; Krafft, J. M.; Bazin, P.; Paganini, M. C.; Giamello, E.; Che, M.; Lauron-Pernot, H.; Costentin, G. *J. Phys. Chem. C* **2010**, *114*, 3008−3016.
(42) Soleymanabadi, H.; Peyghan, A. A. *Comput. Mater. Sci.* **2013**, *79*, 182−186.
(43) Kakkar, R.; Kapoor, P. N.; Klabunde, K. J. *J. Phys. Chem. B* **2006**, *110* (51), 25941−25949.
(44) Kwapien, K.; Sierka, M.; Doebler, J.; Sauer, J. *Chem. Catal. Chem.* **2010**, *2* (7), 819−826.
(45) Wang, C. M.; Wang, Y. D.; Dong, J.; Liu, S.; Xie, Z. K. *Comput. Theor. Chem.* **2011**, *974*, 52−56.
(46) Bailly, M. L.; Costentin, G.; Lauron-Pernot, H.; Krafft, J. M.; Che, M. *J. Phys. Chem. B* **2005**, *109* (6), 2404−2413.
(47) Calatayud, M. *Catal. Today* **2010**, *152* (1−4), 88−92.
(48) Chizallet, C.; Costentin, G.; Che, M.; Delbecq, F.; Sautet, P. *J. Am. Chem. Soc.* **2007**, *129*, 6442.
(49) Cornu, D.; Guesmi, H.; Krafft, J. M.; Pernot, H. *J. Phys. Chem. C* **2012**, *116* (11), 6645−6654.
(50) Cornu, D.; Petitjean, H.; Costentin, G.; Guesmi, H.; Krafft, J. M.; Lauron-Pernot, H. *Phys. Chem. Chem. Phys.* **2013**, *15*, 19870−19871.
(51) Chizallet, C.; Costentin, G.; Lauron-Pernot, H.; Che, M.; Bonhomme, C.; Maquet, J.; Delbecq, F.; Sautet, P. *J. Phys. Chem. C* **2007**, *111*, 18279−18287.
(52) Chizallet, C.; Costentin, G.; Lauron Pernot, H.; Krafft, J. M.; Che, M.; Delbecq, F.; Sautet, P. *J. Phys. Chem. C* **2008**, *112*, 19710−19717.
(53) Chizallet, C.; Costentin, G.; Lauron-Pernot, H.; Krafft, J. M.; Che, M.; Delbecq, F.; Sautet, P. *J. Phys. Chem. C* **2008**, *112*, 16629−16637.
(54) Kresse, G.; Hafner, J. *Phys. Rev. B* **1993**, *47* (1), 558−561.
(55) Kresse, G.; Furthmuller, J. *Comput. Mater. Sci.* **1996**, *6* (1), 15−50.
(56) Perdew, J. P.; Wang, Y.; Engel, E. *Phys. Rev. Lett.* **1991**, *66* (4), 508−511.
(57) Perdew, J. P.; Chevary, J. A.; Vosko, S. H.; Jackson, K. A.; Pederson, M. R.; Singh, D. J.; Fiolhais, C. *Phys. Rev. B* **1992**, *46* (11), 6671−6687.
(58) Blochl, P. E.; Jepsen, O.; Andersen, O. K. *Phys. Rev. B* **1994**, *49* (23), 16223−16233.
(59) Henkelman, G.; Uberuaga, B. P.; Jonsson, H. *J. Chem. Phys.* **2000**, *113* (22), 9901−9904.

(60) E, W.; Ren, W.; Vanden-Eijnden, E. *Phys. Rev. B* **2002**, *66* (5), 052301/1−052301/4.
(61) Fleurat-Lessard, P.; Dayal, P.. Code freely available at: http://perso.ens-lyon.fr/paul.fleurat-lessard/ReactionPath.html.
(62) Loffreda, D. *Surf. Sci.* **2006**, *600* (10), 2103−2112.
(63) Boudart, M.; Djega-Mariadassou, G. *Kinetics of Heterogeneous Catalytic Reactions*; Princeton University Press: Princeton, NJ, 1984; pp 1−240.
(64) Savio, L.; Smerieri, M.; Orzelli, A.; Vattuone, L.; Rocca, M.; Finocchi, F.; Jupille, J. *Surf. Sci.* **2010**, *604* (3−4), 252−257.
(65) Carrasco, E.; Brown, M. A.; Sterrer, M.; Freund, H. J.; Kwapien, K.; Sierka, M.; Sauer, J. *J. Phys. Chem. C* **2010**, *114* (42), 18207−18214.